Multifunctional composite crystal $Cu_xV_4O_{11}$ ($x \approx 2.2$)

Masashige Onoda[1] and Mitsuko Onoda[2]
[1]*Institute of Physics, University of Tsukuba, Tennodai, Tsukuba 305-8571, Japan*
[2]*National Institute for Materials Science, Namiki, Tsukuba 305-0044, Japan*
(Received 1 December 2005; revised manuscript received 30 January 2006; published 13 March 2006; publisher error corrected 5 April 2006)

The crystal structure of the incommensurately modulated system $Cu_xV_4O_{11}$ with $x \approx 2.2$ has been determined in terms of a composite model of $Cu_xV_4O_{11}$ substructure and Cu subchain with different b constants for each monoclinic cell of *Cm*. The effective cation valences and the g factors obtained from the electron spin resonance suggest that the significantly modulated Cu chain in the $Cu_xV_4O_{11}$ substructure is mainly responsible for the Fermi-liquid-like transport between 120 and 340 K, while another Cu chain has an almost empty band. This composition indicates a large thermoelectric power due to the carrier mass enhancement, which might be regarded as a new candidate for thermoelectric devices. This system has also been known useful as a metallic cathode for high-capacity rechargeable batteries, which may be understood in the characteristic framework of composite structure.

DOI: 10.1103/PhysRevB.73.104108 PACS number(s): 61.44.Fw, 61.66.Fn, 71.30.+h, 76.30.Fc

I. INTRODUCTION

The transition-metal ternary oxides and the nonstoichiometric bronzes have aroused considerable interest from both, the basic science and applied viewpoints. For example, many of low-dimensional oxides with partially filled d orbitals, which contain high-T_c oxides and the related ones,[1] have been investigated to clarify properties of correlated electron systems and quantum spin-fluctuation systems. They are also utilized as various functional materials such as thermoelectric devices[2] or rechargeable lithium batteries.[3,4] These basic and applied properties are essentially related to the structures formed by the linkage of rigid units such as the TO_6 octahedra or TO_4 tetrahedra, where T is a transition-metal atom.

This work is pointed at $Cu_xV_4O_{11}$ isolated by Galy and Lavaud.[5] The crystal of $x=1.8$ was monoclinic with space group *Cm*, and the lattice constants were expressed as $a=15.38$, $b=3.61$, $c=7.37$ Å, and $\beta=102.0°$. There exist four crystallographically independent V sites and two inequivalent Cu ones. Sharing both edges and corners, distorted VO_6 octahedra form the V_4O_{11} sheets in the *ab* plane, which are separated by a Cu ion layer. However, this model corresponds to an average structure, because incommensurate reflections or diffuse streaks are observed depending on the Cu concentration and temperature.[6]

It is known that $Cu_xV_4O_{11}$ has several modulation patterns.[7–9] The structure for $x=2.12$ was proposed by Kato *et al.* using the superspace group $Cm(0,\gamma,0)[\gamma=0.2285]$ with lattice constants of $a=15.3004$, $b=3.60866$, $c=7.33566$ Å, and $\beta=101.851°$ (Ref. 7). This is basically similar to the structure described above. The Cu ions are accommodated within two kinds of tunnels. The tetrahedral Cu sites in one tunnel are occupied almost at random. The occupancies and y coordinates of those in the other tunnel are modulated so as to keep appropriate Cu-Cu distances. The positional modulation of V and O sites is expressed as a slight wavy deformation of the V_4O_{11} sheet as a whole. Recently, the structure for $x=2.33$ was determined by Rozier and Lidin using a three-part composite model associated with the V_4O_{11} substructure and with each of the two Cu sites.[9] This composition is not monoclinic but triclinic. Here, the lattice constants for the V_4O_{11} subsystem are described as $a=15.280(3)$, $b_1=3.616(1)$, $c=14.674(3)$ Å, $\alpha=90.0$, $\beta=101.95(3)$, and $\gamma=90.0°$, and the b constants for the two remaining Cu subsystems are $b_2=2.964(1)$ Å and $b_3=3.257(1)$ Å.

Magnetic resonance studies for $Cu_xV_4O_{11}$ suggested that this system has quasi-one-dimensional transport properties and a charge-transfer transition at around room temperature may occur for some Cu concentrations, and both cations of Cu and V are in mixed-valent states.[6] A recent study of the electronic properties for $x \approx 2.33$ also revealed the presence of mixed valence in both Cu and V, although no phase transition was detected.[10]

This work describes the crystal structure and electronic properties of $Cu_xV_4O_{11}$ revealed through measurements of x-ray four-circle diffraction, electron spin resonance (ESR), electrical resistivity, and thermoelectric power and brings the potentially useful properties in this system to light. The experimental details are given in Sec. II. Section III A depicts that $Cu_xV_4O_{11}$ with $x \approx 2.2$ is a composite crystal consisting of the CuV_4O_{11} substructure and the $(x-1)$Cu subchain with mixed-valent states for Cu and V, which is not so complicated as in the recent model.[9] In Sec. III B, the results of ESR and transport properties are discussed referring to the structural details, and in Sec. III C, several functions such as thermoelectric devices and rechargeable batteries are pointed out on the basis of structural and electronic aspects clarified here. Finally, Sec. IV is devoted to a conclusion for the multifunctional composite crystal system of $Cu_xV_4O_{11}$.

II. EXPERIMENTS

Polycrystalline specimens of $Cu_xV_4O_{11}$ with nominal compositions of $2.0 \leqslant x \leqslant 2.5$ were prepared by the solid-state reaction. First, Cu_2O (99.9% purity) was heated in

vacuum at 973 K for 10 h and V_2O_5 (99.99 %) was dried at 473 K. Mixtures of Cu_2O, $(x-2)$Cu (99.9 %), and $2V_2O_5$ were pressed into pellets and heated in vacuum for 10 h at temperatures between 883 and 843 K depending on x, ground, and retreated for 20 h. The single crystals were also prepared by a Bridgman method with the above mixtures.

The electron-probe microanalysis (EPMA) was performed to estimate the Cu/V ratio using a JEOL JAX-8621. The x-ray powder diffraction patterns were taken with Cu$K\alpha$ radiation at room temperature using a Rigaku RAD-IIC diffractometer. The x-ray four-circle diffraction measurements were done at 293 K on a Rigaku AFC-5R diffractometer with graphite-monochromated Mo$K\alpha$ radiation and the temperature dependence of the lattice constants at temperatures between 90 and 350 K was obtained using Enraf-CAD4 diffractometer with graphite-monochromated Cu$K\alpha$ radiation. The four-terminal electrical resistivity and the thermoelectric power were measured with a dc method at temperatures below 500 and 350 K, respectively. The ESR measurements for the polycrystalline specimens were performed at 9.2 GHz using a JEOL spectrometer below 360 K.

III. RESULTS AND DISCUSSION

A. Crystal structure

The Cu concentrations for the polycrystalline specimens with nominal value less than 2.3 agree roughly with those estimated from EPMA. In the subsequent discussion, the Cu concentration determined with EPMA is used. For the range of $2.2 \leqslant x \leqslant 2.37(4)$, the x-ray powder diffraction patterns almost correspond to those calculated on the basis of the average structure. The upper limit of Cu concentration is consistent with the result in Ref. 11 within an experimental error. On the other hand, for the single crystals prepared here, the actual Cu concentration is estimated to be $x \approx 2.2$ irrespective of the nominal composition. The scanning electron microscopy indicates the limitation of Cu concentration for the single crystals to be compensated by an appearance of other phases, such as the Cu metal and the bronze CuV_2O_5.

The single-crystal specimens have incommensurate reflections at wave vector $\boldsymbol{q} \approx 0.16\boldsymbol{b}^*$ and diffuse streaks at $\boldsymbol{q} = \boldsymbol{c}^*/3$ with respect to the cell with $a=15.287(1)$, $b=3.599(1)$, $c=7.293(1)$ Å, and $\beta=102.69(1)^\circ$ (Refs. 6 and 8). The size of $\boldsymbol{q}$ is constant within an error of 0.002 between 90 and 300 K. This anomaly is ascribed to an incommensurability of the Cu-Cu distances in the chain for the lattice constant of the b axis in the V_4O_{11} sheets. The structure for the single-crystal specimens determined in the averaged form with space group *Cm* using TEXSAN (Refs. 8 and 12) is almost similar to that of Ref. 10, although in the present crystal, the Cu(1) atom is assumed to be located on a mirror plane with a full occupation. For the Cu(2) site, an electron density appears to be distributed significantly along the b direction, which is of course caused by neglecting the incommensurate reflections and may correspond to the published result. This analysis provides the Cu(2) concentration of 1.16(7) per CuV_4O_{11}, which leads to the chemical formula $Cu_{2.16}V_4O_{11}$, consistent with the EPMA value within the margin of error.

TABLE I. The atomic parameters, isotropic and equivalent isotropic thermal parameters ($U_{iso,eq}$), and the cosine ($A_{x,z}$) and sine (B_y) amplitudes of the Fourier series of the modulation function for $Cu_{2.16}V_4O_{11}$ at 293 K. Here, $U_{iso(eq)}$ is applied to O (Cu and V).

Atom	x	y	z	$U_{eq/iso}$	A_x	B_y	A_z
				Subsystem 1			
Cu(1)	$\frac{1}{2}$	$\frac{1}{2}$	$\frac{1}{2}$	0.132(2)	−0.0035(6)	−0.193(2)	−0.025(1)
V(1)	0.1099(2)	0	0.1559(5)	0.0098(8)	0.0060(5)	0.012(3)	0.023(1)
V(2)	0.3292(3)	0	0.1502(6)	0.021(1)	0.0038(6)	0.000(3)	0.017(1)
V(3)	0.1723(2)	$\frac{1}{2}$	−0.1469(5)	0.0113(8)	−0.0007(5)	0.015(3)	−0.0216(9)
V(4)	0.3895(2)	$\frac{1}{2}$	−0.1485(5)	0.0114(8)	−0.0044(5)	0.005(3)	−0.020(1)
O(1)	0.1366(7)	$\frac{1}{2}$	0.112(2)	0.015(2)	−0.002(2)	−0.013(8)	−0.024(3)
O(2)	0.3139(7)	$\frac{1}{2}$	0.074(2)	0.006(2)	−0.015(1)	0.004(9)	−0.040(2)
O(3)	0.1856(7)	0	−0.068(1)	0.0010(2)	−0.008(1)	−0.006(8)	0.004(3)
O(4)	0.3760(6)	0	−0.092(1)	0.009(2)	0.006(2)	−0.002(9)	0.019(3)
O(5)	−0.001(2)	0	0.007(4)	0.018(1)	0.0037(9)	0.03(2)	0.021(2)
O(6)	0.0848(7)	0	0.362(2)	0.006(2)	0.014(1)	0.034(5)	0.030(2)
O(7)	0.2508(8)	0	0.299(2)	0.013(3)	−0.009(1)	0.044(7)	−0.001(3)
O(8)	0.4314(8)	0	0.305(2)	0.027(3)	0.005(2)	0.026(8)	0.018(4)
O(9)	0.0810(7)	$\frac{1}{2}$	0.705(2)	0.014(2)	−0.004(2)	0.007(8)	−0.023(4)
O(10)	0.2500(8)	$\frac{1}{2}$	0.708(2)	0.013(3)	−0.013(1)	0.029(7)	−0.029(3)
O(11)	0.4129(8)	$\frac{1}{2}$	0.639(2)	0.022(3)	0.005(1)	−0.017(6)	−0.009(4)
				Subsystem 2			
Cu(2)	0.2510(5)	0	0.501(1)	0.074(1)	−0.0022(3)	0.026(5)	0.0749(4)

TABLE II. The anisotropic displacement parameters U_{ij} for $Cu_{2.16}V_4O_{11}$ at 293 K.

Atom	U_{11}	U_{22}	U_{33}	U_{13}
Cu(1)[a]	0.0187(9)	0.369(4)	0.010(2)	0.007(1)
V(1)	0.014(1)	0.002(1)	0.015(2)	0.008(1)
V(2)	0.029(2)	0.006(1)	0.031(2)	0.016(1)
V(3)	0.025(1)	0.002(1)	0.013(1)	0.018(1)
V(4)	0.012(1)	0.009(1)	0.015(1)	0.008(1)
Cu(2)[b]	0.0405(9)	0.161(3)	0.020(2)	0.008(1)

[a]The cosine amplitudes ($A_{U_{11,22,33,13}}$) of the Fourier series of the modulation function are 0.006(3), 0.397(4), −0.006(3), −0.012(2), respectively, and the sine ones ($B_{U_{12,23}}$) are 0.028(5), −0.005(5).
[b]$A_{U_{11,22,33,13}} = -0.014(5), 0.086(7), 0.009(3), -0.002(3)$ and $B_{U_{12,23}} = 0.013(3), -0.072(2)$.

A good agreement between the Cu concentration estimated from EPMA and that obtained in the average structure analysis suggests that a composite crystal model consisting of the CuV_4O_{11} substructure with $b_1 = 3.599(1)$ Å and the Cu(2) chain with $b_2 = 3.097(2)$ Å, each space group being Cm, is suitable. Refinement of this model was performed on the basis of $|F|$ through the program FMLSM (Ref. 13) with σ weight for all of the reflections using modulation function defined by $m(t) = A\cos(2\pi t) + B\sin(2\pi t)$, where $m(t)$ is one of displacement modulations or the modulation in the thermal parameter and t corresponds to the fourth-dimensional coordinate in a superspace and represents the phase of the modulation wave. The reciprocal base vectors of the first part (a^*, b_1^*, c^*) and those of the second part (a^*, b_2^*, c^*) are related to the minimal vector set in reciprocal space $\{a^*, b_1^*, c^*, b_2^*\}$ through the Z matrices, $Z_1 = (1000|0100|0010)$ and $Z_2 = (1000|0001|0010)$.

The atomic parameters finally obtained with the reliability factor $R = 0.066$ and the weighted factor $R_w = 0.043$ for 1755 reflections ($F \geq 3\sigma$), of which 407 reflections come from subsystem 2, are listed in Tables I and II,[14] and the structure is shown in Fig. 1. Selected interatomic bond lengths are presented in Fig. 2 and in Table III. As described before, this structure consists of a V_4O_{11} layer and the Cu atoms located between the layers. The latter atoms have significant positional modulations. The Cu(1) atoms that belong to CuV_4O_{11} substructure have an octahedral coordination or two kinds of tetrahedral coordination depending on positive and negative shifts of y. Taking account of the large amplitude of anisotropic displacement parameter U_{22} (Table II), the Cu(1) atoms may oscillate between two different tetrahedral sites. This significant oscillation may cause the diffuse streak at $\boldsymbol{q} = \boldsymbol{c}^*/3$. On the other hand, the Cu(2) atoms with b constant of 3.097 Å have a triangular or tetrahedral surrounding which mainly depends on the z modulation of Cu(2) site. The V atoms in CuV_4O_{11} substructure are surrounded octahedrally, and the positional modulations for V as well as O are very small as compared with those of Cu atoms. The anisotropic displacement parameters for V and the metal-metal distances presented in Figs. 2(c) and 2(d) and in Table III are in a normal range except for the Cu(1)-Cu(1) distance with a large positional modulation along the b axis.

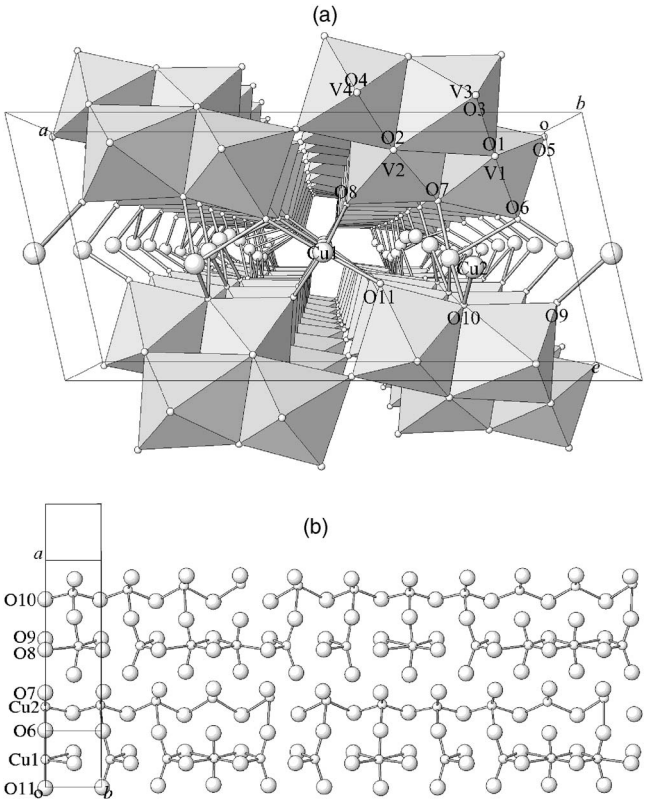

FIG. 1. The crystal structures of $Cu_{2.16}V_4O_{11}$ at 293 K: (a) the projection on the monoclinic ac plane with the polyhedral scheme and (b) the clinographic view of Cu(1) and Cu(2) chains along the b direction.

For understanding of electronic properties, effective valences of Cu and V ions calculated on the basis of the bond-length-bond-strength relation[15,16] are shown in Figs. 2(a) and 2(b), respectively. The Cu(1) and Cu(2) ions are rather close to the states of Cu^{2+} and Cu^{+}, respectively. On the other hand, V ions except V(3) are in a mixed valence of V^{4+} and V^{5+}. The result that the valence of V(3) is slightly larger than 5 may be owing to the structure analysis without consideration of the diffuse streak. However, this result does not affect the following discussion. Thus, both Cu and V ions have d electrons as confirmed in Ref. 6. Considering octahedral field contracted tetragonally along the z' direction with $\boldsymbol{z}' \| 2\boldsymbol{a} - 3\boldsymbol{c}$ on the basis of the Cu(1)-O bond lengths in Fig. 2(a), the ground-state orbital is basically $d_{3z'^2-r^2}$. On the other hand, the V(1) andV(4) ions may have the $d_{x''y''}$-like ground-state wave functions with $\boldsymbol{x}'' \| \boldsymbol{a} + \boldsymbol{c}$ and $\boldsymbol{y}'' \| \boldsymbol{b}$ according to the results in Fig. 2(b). Therefore, the V(1)-V(4) network is roughly approximated with a ladder model that provides a spin-singlet state depending on the ratio of the exchange couplings for the leg and rung directions as often seen in V oxide systems.[17] The transition to the spin-singlet state in V ions at around 300 K for a certain composition[6] would be explained with this model.

The composite crystal model for $x = 2.33$ introduced in Ref. 9, examined through the Z matrices of $Z_1 = (1000|0100|0010)$, $Z_2 = (1000|0102|0010)$, and $Z_3 = (1000|0101|0010)$ with the assumption of the σ matrices

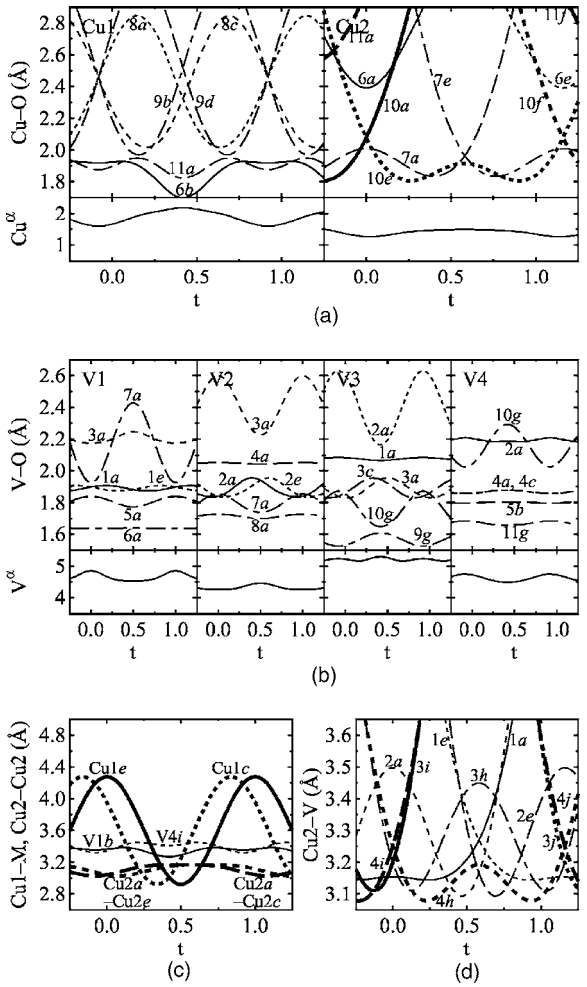

FIG. 2. The interatomic distances and the effective valences for $Cu_{2.16}V_4O_{11}$ at 293 K plotted as a function of the four-dimensional coordinate t: (a) Cu-O distances and Cu valences, (b) V-O distances and V valences, (c) Cu(1) -metal (M) and Cu(2)-Cu(2) distances, and (d) Cu(2)-V distances. Here, symmetry operation codes attached to curves are as follows: (a) x,y,z; (b) $\frac{1}{2}+x$, $\frac{1}{2}+y,z$; (c) $x,1+y,z$; (d) $\frac{1}{2}+x$, $-\frac{1}{2}+y,z$; (e) $x,-1+y,z$; (f) $x,-2+y,z$; (g) $x,y,-1+z$; (h) $x,-1+y,1+z$; (i) $x,y,1+z$; (j) $x,-2+y,1+z$; and (k) $-\frac{1}{2}+x,-\frac{1}{2}+y,z$.

of 0.081, provides similar results with a little large factors of $R=0.083$ and $R_w=0.058$.

B. Magnetic and transport properties

1. Electron spin resonance

The ESR measurements for a polycrystalline specimen with $x=2.23$ at temperatures above 180 K indicate a single Lorentzian having averaged values (g_{av} and W_{av}) for the g factors and the peak-to-peak linewidths of the absorption derivative. At the lower temperature, a powder pattern appears due to the decrease of linewidths that is expected from the uniaxial anisotropy with principal values ($g_{\parallel,\perp}$ and $W_{\parallel,\perp}$) for the g and linewidth, the subscripts $\parallel$ and $\perp$ indicating the directions parallel and perpendicular to the unique axis, respectively. The temperature dependences of the g factors and linewidths are shown in Figs. 3(a) and 3(b), respectively. It is found that the space-averaged values of $g_{\parallel,\perp}$ and $W_{\parallel,\perp}$ continuously connect with g_{av} and W_{av} for the single Lorentzian. Above $T_{ESR1}\simeq 340$ K, g is smaller than 2 and temperature independent, while below T_{ESR1}, it increases positively and becomes larger than 2, and then saturates at $T_{ESR2}\simeq 120$ K. The linewidths at temperatures above T_{ESR1} and below T_{ESR2} are almost temperature independent, while between T_{ESR1} and T_{ESR2}, they exhibit a broad maximum.

The change of the sign for the g shift $\Delta g\simeq g-2$ apparently indicates that the ESR active ions are like a V^{4+} above T_{ESR1} and Cu^{2+} below T_{ESR1} according to the theory of spin-orbit interactions.[6] Another possible origin is a dynamical Jahn-Teller effect accompanied by a significant reduction of orbital momentum.[18] In order to determine which of these interpretations is more appropriate, further experiments are necessary. At least, it is postulated that Cu^{2+}-like ions in the Cu(1) site mainly contribute to ESR signals below T_{ESR1}. On the basis of the wave function of Cu^{2+} described in Sec. III A, a small positive shift from a free electron value for $g_{\parallel}$

TABLE III. The selected interatomic distances (Å) between the V ions for $Cu_{2.16}V_4O_{11}$ at 293 K with symmetry operation codes defined in Fig. 2.

	Minimum	Maximum
Corner-shared path		
V(1)^a-V(1)^{c,e}	3.559(10)	3.640(10)
V(1)^a-V(4)^k	3.577(13)	3.633(13)
V(2)^a-V(2)^{c,e}	3.599(11)	3.601(2)
V(3)^a-V(3)^{c,e}	3.545(10)	3.654(10)
V(4)^a-V(4)^{c,e}	3.582(11)	3.617(11)
Edge-shared path		
V(1)^a-V(2)^a	3.338(14)	3.387(13)
V(1)^a-V(3)^{a,e}	3.122(9)	3.188(9)
V(2)^a-V(3)^{a,e}	3.362(7)	3.394(6)
V(2)^a-V(4)^{a,e}	3.088(9)	3.147(9)

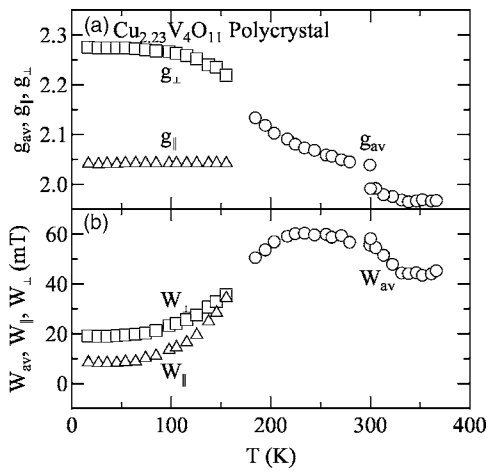

FIG. 3. The temperature dependences of (a) the g factors and (b) the peak-to-peak linewidths of the absorption derivatives for the polycrystalline specimen of $Cu_{2.23}V_4O_{11}$.

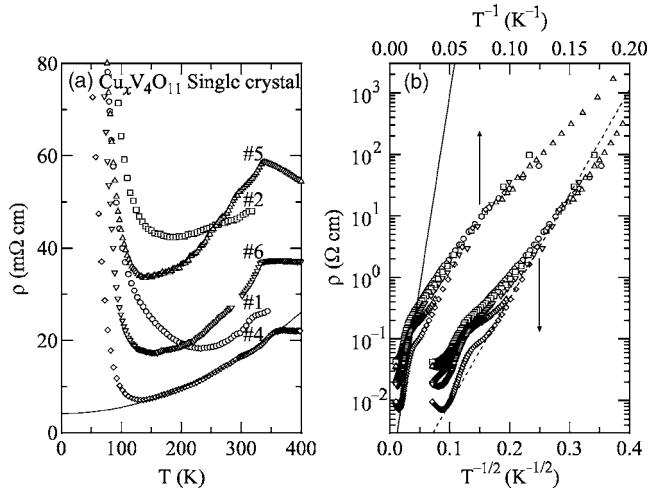

FIG. 4. (a) The electrical resistivities as a function of temperature for the single-crystal specimens of $Cu_xV_4O_{11}$ and (b) the low-temperature data against $T^{-1/2}$ (the bottom abscissa) and T^{-1} (the top abscissa). Here, the solid curve in (a) indicates a fit to Eq. (1), and the solid and dotted lines in (b) are those to Eqs. (2) and (3), respectively.

below T_{ESR2} may be attributed to the zero-point motion in the Jahn-Teller effect.[19] In addition, the large positional modulation along the b axis is also responsible for the shift of $g_{\|}$.

2. Electrical resistivity and thermoelectric power

The electrical resistivities ρ against temperature for several single-crystal specimens are shown in Fig. 4(a), and those against T^{-1} and $T^{-1/2}$ are in Fig. 4(b). The data are sample dependent irrespective of the similar composition and range from 10 to 50 mΩ cm at 300 K. Above $T_{\rho 1} \simeq 340$ K, the resistivity increases gradually or almost constant with decreasing temperature, between $T_{\rho 1}$ and the sample-dependent $T_{\rho 2}$=120– 220 K, it exhibits a metallic transport, and at around $T_{\rho 2}$, a crossover from metallic to semiconducting states takes place. Here, $T_{\rho 1,\rho 2}$ may agree with $T_{ESR1,ESR2}$ presented in the previous section, respectively. It is noted that for the Cu concentration near to 2.33 corresponding to the composite model in Ref. 9, the electronic properties are basically semiconducting. A subsequent discussion is for the data of sample No. 4 with the smallest resistivity.

The resistivities between $T_{\rho 1}$ and $T_{\rho 2}$ approximately follow the Fermi-liquid relation[20]

$$\rho = \rho_0 + CT^2, \tag{1}$$

where the residual resistivity ρ_0 and a constant C are 4.2 mΩ cm and 0.14 μΩ cm K^{-2}, respectively, for the solid curve in Fig. 4(a). Between $T_{\rho 2}$ and 60 K, the empirical formula of

$$\rho \propto \exp(E_\rho/T) \tag{2}$$

may be applied with the apparent activation energy $E_\rho = 2.9 \times 10^2$ K as shown by the solid line in Fig. 4(b). At the lower temperatures, the resistivities nearly follow the variable-range hopping (VRH) transport of the form

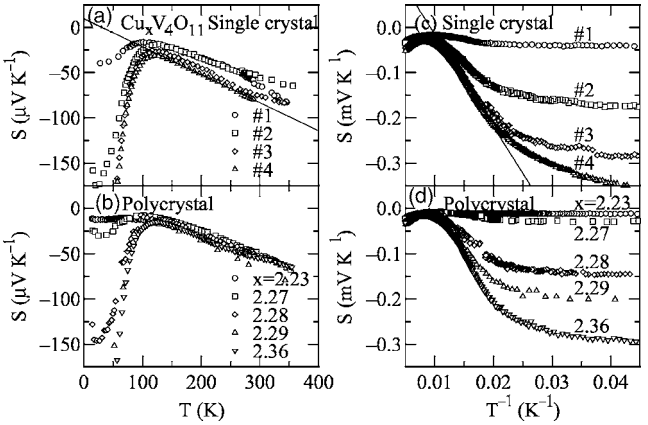

FIG. 5. The temperature dependences of the thermoelectric powers for (a), (c) the single-crystal and (b), (d) polycrystalline specimens of $Cu_xV_4O_{11}$, where (a), (b) and (c), (d) indicate the data against T and T^{-1}, respectively. Here, the solid lines in (a) and (c) denote fits to Eqs. (4) and (5), respectively.

$$\rho \propto \exp\sqrt{T_0/T}, \tag{3}$$

with $T_0 = 1.5 \times 10^3$ K as indicated by the dotted line in Fig. 4(b). This exponent suggests that the transport is either Efros-Shklovskii (ES) type[21,22] or Mott type.[23] The former originates from a soft Coulomb gap Δ due to Coulomb interactions between the localized electrons and the latter type is for weakly coupled chains[24] or finite chains.[25,26] At temperatures lower than a certain critical temperature T_{ES}, the ES mechanism may be appropriate and T_0 is given by $T_0 \approx 12\Delta^2/T_{ES}$.[22] Using $T_{ES} \approx 50$ K, we obtain the reasonable result of $\Delta \approx 80$ K from the above T_0.

Figures 5(a) and 5(c) indicate the thermoelectric powers S against temperature and $1/T$ for the single-crystal specimens, respectively, and Figs. 5(b) and 5(d) are for the polycrystalline specimens. The results for single crystals labeled Nos. 1–4 seem to correspond to those for polycrystals with x =2.23–2.36, respectively. Here, it should be noted that grain-boundary resistances for the polycrystalline specimens are generally considered to have less influence on the data as compared with that on the resistivity. All of the data have a negative sign, indicating an electron carrier, and above $T_S \simeq 120$ K corresponding to both T_{ESR2} and $T_{\rho 2}$, they follow a metallic T-linear dependence

$$S = S_0 - \left. \frac{\pi^2 k^2 T}{3e} \frac{\mathrm{d} \ln \sigma(E)}{\mathrm{d}E} \right|_{E_F}, \tag{4}$$

where S_0 is a constant, k is the Boltzmann constant, σ is a conductivitylike function of electron energy E, and E_F is the Fermi energy. The solid line for sample No. 4 in Fig. 5(a) is drawn with $S = (9.6 - 0.31T)$ μV K^{-1}. The reason why the absolute magnitudes of the thermoelectric powers are larger than those of simple metals may be principally due to the enhancement of carrier mass or the reduction of the Fermi energy as suggested from the resistivity results.

Below T_S, the thermoelectric power depends on the single-crystal specimen and the composition of the polycrystalline specimens. The data with x=2.23 remain constant

($S \simeq -10\ \mu V\ K^{-1}$). With increasing the Cu concentration of polycrystalline specimens, the rapid downturn becomes significant, indicating that the metal-semiconductor crossover is enhanced. According to the relation between S and the apparent gap E_S shown below,

$$S = S_0 - eE_S/T, \tag{5}$$

E_S is estimated to be 2.4×10^2 K on the basis of the solid line for sample No. 4 between T_S and 50 K in Fig. 5(c), which agrees roughly with the gap for the resistivity, suggesting a band-semiconductor-like conduction. However, the sample dependence of E_ρ is not always consistent with that of E_S; for example, the resistivity for sample No. 1 exhibits a gaplike behavior, whereas the thermoelectric power does not. This is because the distribution of Cu concentration for the single crystals is a little inhomogeneous. At temperatures below 50 K, the temperature dependence of thermoelectric power deviates from Eq. (5) and becomes constant. This temperature-independent behavior seems to be consistent with the ES model that provides a nonzero constant as temperature approaches to zero.[22]

C. Functions for composite crystals

The resistivity of 10^1 mΩ cm and the thermoelectric power of $10^2\ \mu V\ K^{-1}$ provide a power factor 10^{-4} W m^{-1} K^{-2}. This factor is a little smaller than that of Na_xCoO_2 regarded as thermoelectric materials[2] which directly convert heat energy into electrical energy. However, the magnitude of resistivity still stands improvement considering its sample dependence, so that $Cu_xV_4O_{11}$ might become a new candidate for such a device.

For an application to rechargeable Li batteries with the use of transition-metal oxides, structural instabilities or phase separations for undergoing intercalation and deintercalation with Li ions often give rise to a serious problem such as a lowering of discharge-charge cycle performance. This problem would be settled using a structural incommensurability between the Li (guest) site and the host lattice. In effects, electrochemical measurements with $Cu_xV_4O_{11}$ cathodes have shown a high capacity of 2.5×10^2 mA h g^{-1}, corresponding to 5Li per $Cu_xV_4O_{11}$,[27] which is comparable with the value for $Ag_2V_4O_{11}$ that has been used as the primary power source for implantable biomedical devices.[3,28] Here, the discharge and charge processes are principally related to the reduction and oxidation for the localized V_4O_{11} layers, respectively. The Li ions doped to the $Cu_xV_4O_{11}$ host are considered to reside in the aperture formed by the significant displacement of Cu(2) ions in the *ac* plane as described in Sec. III A.

IV. CONCLUSIONS

The structure analysis of the incommensurately modulated system $Cu_xV_4O_{11}$ with $x \approx 2.2$ indicates that this composition at 293 K is a composite crystal consisting of CuV_4O_{11} substructure and Cu subchain with different b constants for each monoclinic cell of *Cm*. Two kinds of phase transitions take place at $T_{ESR1} \simeq T_{\rho 1} \simeq 340$ K and at $T_{ESR2} \simeq T_{\rho 2} \simeq T_S \simeq 120$ K. The effective cation valences and the g factors obtained from ESR suggest that the significantly modulated Cu chain in the CuV_4O_{11} substructure is more magnetic and it may be predominantly responsible for the Fermi-liquid-like transport between 120 and 340 K, while another Cu chain is less magnetic and has an almost empty band. The V ions form the mixed-valent states of V^{4+} and V^{5+} as expected from the chemical formula, and the pairs of V(1) and V(4) may be approximated with the rung dimer in the ladder from the symmetry of ground-state d orbital in V ions.

The present composition indicates a large thermoelectric power due to the carrier mass enhancement, which might be regarded as a new candidate of thermoelectric devices. The nonmetallic behavior below 120 K is likely due to the order of Cu chains and that at the lower temperature is mainly originated from the soft Coulomb gap. Another nonmetallic transition at 340 K may be caused by the charge-transfer-like transition accompanied by a gap for V ions and/or the more significant disorder of Cu chains. This system has also been known useful as a metallic cathode for high-capacity rechargeable batteries, which is successfully understood in the framework of composite structure.

This work suggests that $Cu_xV_4O_{11}$ with $x \approx 2.2$ has the metallic Cu chain between the localized V_4O_{11} layers, which may remind us the Little's proposal for the excitonic superconductivity.[29] In order to establish various characteristics for the metallic mixed-valent composite crystal system described above, further investigations are needed. It is also necessary to explore properties of the lithiated system with the discharged state from many-sided viewpoints.

ACKNOWLEDGMENTS

The first author is grateful to H. Nagasawa and S. Kagoshima for information on the structural properties. He is also thankful to K. Nichogi for collaboration of an ionic battery research and to M. Kohno for help with ESR and transport measurements.

*Electronic address: onoda@sakura.cc.tsukuba.ac.jp

[1] For recent topic, see K. Takada, H. Sakurai, E. Takayama-Muromachi, F. Izumi, R. A. Dilanian, and T. Sasaki, Nature (London) **422**, 53 (2003).

[2] I. Terasaki, Y. Sasago, and K. Uchinokura, Phys. Rev. B **56**, R12685 (1997).

[3] E. S. Takeuchi, J. Power Sources **54**, 115 (1995).

[4] M. Onoda, S. Miyasaka, T. Mutoh, and K. Nichogi, J. Phys.:

Condens. Matter **17**, 4057 (2005) and references therein.
[5] J. Galy and D. Lavaud, Acta Crystallogr., Sect. B: Struct. Crystallogr. Cryst. Chem. **27**, 1005 (1971).
[6] Y. Saito, M. Onoda, and H. Nagasawa, J. Phys. Soc. Jpn. **61**, 3865 (1992) and references therein.
[7] K. Kato, K. Kosuda, Y. Saito, and H. Nagasawa, Z. Kristallogr. **211**, 522 (1996).
[8] M. Onoda and H. Nagasawa (unpublished).
[9] P. Rozier and S. Lidin, J. Solid State Chem. **172**, 319 (2003).
[10] P. Rozier, J. Galy, G. Chelkowska, H.-J. Koo, and M.-H. Whangbo, J. Solid State Chem. **166**, 382 (2002).
[11] P. Rozier, C. Satto, and J. Galy, Solid State Sci. **2**, 595 (2000).
[12] TEXSAN, Crystal Structure Analysis Package, Molecular Structure Corporation, The Woodlands, TX, 1992.
[13] K. Kato, Acta Crystallogr., Sect. A: Found. Crystallogr. **50**, 351 (1994).
[14] See EPAPS Document No. E-PRBMDO-73-070610 for the observed and calculated structure factor tables of $Cu_{2.16}V_4O_{11}$ at 293 K. This document can be reached via a direct link in the online article's HTML reference section or via the EPAPS homepage (http://www.aip.org/pubservs/epaps.html).
[15] W. H. Zachariasen, J. Less-Common Met. **62**, 1 (1978).
[16] I. D. Brown and D. Altermatt, Acta Crystallogr., Sect. B: Struct. Sci. **41**, 244 (1985).
[17] M. Onoda, T. Ohki, and Y. Uchida, J. Phys.: Condens. Matter **16**, 7863 (2004) and references therein.
[18] T. Yamaguchi and H. Kamimura, J. Phys. Soc. Jpn. **33**, 953 (1972).
[19] A. Abragam and B. Bleaney, *Electron Paramagnetic Resonance of Transition Ions* (Clarendon, Oxford, 1970).
[20] K. Kadowaki and S. B. Woods, Solid State Commun. **58**, 507 (1986).
[21] A. L. Efros and B. I. Shklovskii, J. Phys. C **8**, L49 (1975).
[22] M. J. Burns and P. M. Chaikin, J. Phys. C **18**, L743 (1985).
[23] N. F. Mott, J. Non-Cryst. Solids **1**, 1 (1968).
[24] E. P. Nakhmedov, V. N. Prigodin, and A. N. Samukhin, Sov. Phys. Solid State **31**, 368 (1989).
[25] W. Brenig, G. H. Döhler, and H. Heyszenau, Philos. Mag. **27**, 1093 (1973).
[26] R. A. Serota, R. K. Kalia, and P. A. Lee, Phys. Rev. B **33**, 8441 (1986).
[27] K. Nichogi (personal communication).
[28] M. Onoda and K. Kanbe, J. Phys.: Condens. Matter **13**, 6675 (2001).
[29] W. A. Little, Phys. Rev. **134**, A1416 (1964).